Toxoplasma Actin Is Required for Efficient Host Cell Invasion

Lisa L. Drewry, L. David Sibley

Department of Molecular Microbiology, Washington University School of Medicine, St. Louis, Missouri, USA

ABSTRACT Apicomplexan parasites actively invade host cells using a mechanism predicted to be powered by a parasite actin-dependent myosin motor. In the model apicomplexan *Toxoplasma gondii*, inducible knockout of the actin gene, *ACT1*, was recently demonstrated to limit but not completely abolish invasion. This observation has led to the provocative suggestion that *T. gondii* possesses alternative, ACT1-independent invasion pathways. Here, we dissected the residual invasive ability of Δ*act1* parasites. Surprisingly, we were able to detect residual ACT1 protein in inducible Δ*act1* parasites as long as 5 days after *ACT1* deletion. We further found that the longer Δ*act1* parasites were propagated after *ACT1* deletion, the more severe an invasion defect was observed. Both findings are consistent with the quantity of residual ACT1 retained in Δ*act1* parasites being responsible for their invasive ability. Furthermore, invasion by the Δ*act1* parasites was also sensitive to the actin polymerization inhibitor cytochalasin D. Finally, there was no clear defect in attachment to host cells or moving junction formation by Δ*act1* parasites. However, Δ*act1* parasites often exhibited delayed entry into host cells, suggesting a defect specific to the penetration stage of invasion. Overall, our results support a model where residual ACT1 protein retained in inducible Δ*act1* parasites facilitates their limited invasive ability and confirm that parasite actin is essential for efficient penetration into host cells during invasion.

IMPORTANCE The prevailing model for apicomplexan invasion has recently been suggested to require major revision, based on studies where core components of the invasion machinery were genetically disrupted using a Cre-Lox-based inducible knockout system. For the myosin component of the motor thought to power invasion, an alternative parasite myosin was recently demonstrated to functionally compensate for loss of the primary myosin involved in invasion. Here, we highlight a second mechanism that can account for the surprising ability of parasites to invade after genetic disruption of core invasion machinery. Specifically, residual actin protein present in inducible knockout parasites appears able to support their limited invasion of host cells. Our results have important implications for the interpretation of the apicomplexan invasion model and also highlight significant considerations when analyzing the phenotypes of inducible knockout parasites generated using Cre-Lox technology.

*T*oxoplasma gondii is a model for studying the gliding motility and active host cell invasion that are characteristic of many members of the *Apicomplexa* phylum of eukaryotic parasites. During gliding, *T. gondii* tachyzoites secrete transmembrane adhesins at their apical (anterior) end (1). Rearward trafficking of these adhesins is predicted to generate the force that propels the parasite forward (1). A parasite actin-dependent myosin motor is thought to power this process (2, 3). According to the currently prevailing model for gliding and invasion, the force generated by gliding motility can be exploited to power movement along a surface substrate, invasion into a host cell or across biological barriers, or egress out of a host cell (1).

When used for invasion, gliding motility is coupled to secure apical attachment to a host cell. Once apically attached, parasites squeeze through a tight constriction referred to as the moving junction (MJ) and penetrate into the host cell (4, 5). Invasion is rapid, typically completing in less than a minute (6), but contains several distinct stages (7). The first committed step is apical attachment to a host cell, with contact mediated by sequential secretion of proteins from the microneme and rhoptry organelles (8). Penetration through an MJ, containing a complex of micronemal

and rhoptry neck proteins (9, 10), leads to invagination of the host cell plasma membrane. Ultimately, pinching off of the host membrane results in internalization (1, 7).

A role for parasite actin in invasion was first suggested by studies demonstrating the ability of the actin polymerization inhibitor cytochalasin D (CytD) to block invasion (11). *T. gondii* contains only one actin gene, *ACT1* (12). Subsequent studies showed that CytD sensitivity is abolished in parasites bearing a CytD resistance-conferring $act1^{A136G}$ allele but is unaffected by the introduction of a CytD-resistant actin allele in host cells (2). Together, these results were interpreted to indicate that CytD acts primarily and specifically on *T. gondii* ACT1 and to support a role for ACT1 polymerization as necessary for invasion.

Although CytD mutant analysis suggests that parasite ACT1 is the predominant actin required for invasion, host cell actin may also contribute to invasion. In support of this idea, several recent studies have highlighted rearrangements of host cell cortical actin during invasion and proposed a possible secondary role for host actin during invasion (13, 14). In addition, the development of a Cre-Lox-based inducible knockout system for *T. gondii* facilitated the generation of inducible *ACT1* knockout parasites (15). Studies

using these inducible Δ*act1* parasites have demonstrated low levels of invasion as many as 4 days following *ACT1*^f excision (15, 16). This result has been suggested as evidence for the presence of an alternative, ACT1-independent invasion pathway in *T. gondii* (15, 16). Under this model, it was suggested that the essential function of ACT1 is to enable segregation of the apicoplast organelle among daughter cells (15) rather than to participate in invasion. Additionally, based on noted defects in MJ formation by these inducible Δ*act1* parasites, it was proposed that any role for ACT1 in invasion occurs during early attachment stages (16) rather than in powering penetration, as was previously theorized (2).

Additional studies used the same Cre-Lox technology to generate stable parasite lines with deletions of the myosin *MYOA* (15, 16) and micronemal MJ component *AMA1* (17). As *T. gondii* is an obligate intracellular parasite, the viability of these knockout mutants clearly demonstrates that *MYOA* and *AMA1* are not essential for invasion, as had been previously theorized (3, 18). Further work has demonstrated that paralogs can functionally compensate for *MYOA* and *AMA1* loss (19, 20). A similar scenario is unlikely to apply to *ACT1*, as the *T. gondii* genome does not encode any clear ACT1 paralogs. However, all studies so far agree that, unlike *MYOA* and *AMA1*, *ACT1* appears to be an essential gene in *T. gondii*, in that no viable null clones are able to grow as stable lines (15, 16). Accordingly, ACT1 function can only be analyzed in parasites that have been depleted of ACT1, rather than in true phenotypic nulls. Notably, *T. gondii* ACT1 polymerizes isodesmically, with no apparent critical concentration required to support polymerization (21, 22). It is thus possible that even very small amounts of ACT1 retained in inducible Δ*act1* parasites could be sufficient to support ACT1 polymerization. Unfortunately, to date, studies using inducible Δ*act1* parasites have only cursorily examined these mutants for residual ACT1 (15, 16) and have failed to rigorously quantify the residual ACT1 present in these mutants. It thus remains uncertain how closely inducible Δ*act1* parasites approximate true phenotypic nulls or whether ACT1 polymerization is likely to be entirely ablated in such mutants.

Here, we sought to analyze in more detail the invasion of inducible Δ*act1* parasites. In particular, we focused on evaluating (i) how severely and consistently ACT1 is depleted in Δ*act1* parasites, (ii) how robustly invasion and other forms of gliding motility are able to continue in Δ*act1* parasites, and (iii) how ACT1 depletion affects specific stages of invasion. In total, our results highlight the importance of residual ACT1 in evaluating the phenotype of inducibly Δ*act1* parasites and confirm that ACT1 is specifically required at the penetration stage of invasion.

RESULTS

Effect of *ACT1* knockout on parasite motility. To investigate the relationship between ACT1 protein abundance and function, we assayed actin-dependent motility using a previously described inducible knockout strain called *ACT1*^f-1 (15). We compared the ability of parasites to invade host cells, egress from host cells, and glide on serum-coated glass 2 days after *ACT1* disruption. As rapamycin induction achieves only low rates of *ACT1*^f excision in parasites of this strain, we analyzed the invasion competence of Δ*act1* parasites by tracking their abundance in a mixed population of *ACT1*^f intact and Δ*act1* parasites (yellow fluorescent protein [YFP] positive) before and after invasion of host cells. To do this, we modified a standard immunofluorescence-based invasion as-

say (23) to stain parasites based on whether they were YFP positive or negative, in addition to determining whether they were intracellular or extracellular. This modification allows for the classification of every parasite as intracellular or extracellular based on permeabilization-selective staining and as Δ*act1* or *ACT1*^f intact based on YFP expression. When invasion was analyzed in this manner, Δ*act1* parasites were found to be consistently underrepresented among intracellular parasites relative to their abundance in the input population, indicating a strong invasion defect (Fig. 1A). Similarly, when egress induced by the calcium ionophore A23187 was observed by time-lapse video microscopy, Δ*act1* vacuoles overwhelmingly failed to egress from host cells, indicating a strong egress defect compared to the phenotype of *ACT1*^f intact parasites (Fig. 1B). Δ*act1* parasites were also observed to glide less frequently on serum-coated coverslips than *ACT1*^f intact parasites, and although less efficient, *ACT1* knockout parasites were capable of all three motility patterns (Fig. 1C).

Generation of a new strain with inducible *ACT1* knockout. The low excision rate of the ACT1^f-1 strain hinders rigorous quantification of these mutants' phenotypes. Therefore, to facilitate further work with inducible Δ*act1* parasites, we used the same strategy employed previously (15) to generate additional *ACT1*^f clones. Briefly, in this strategy, the native *ACT1* allele was replaced by double homologous recombination with an exogenous copy in which the *ACT1* coding sequence is flanked immediately 5′ and 3′ by LoxP sites and followed downstream by a YFP reporter and selectable HXPGRT marker (see Fig. S1 in the supplemental material). The native *ACT1* promoter is retained so that Cre-mediated recombination at the LoxP sites creates a locus where *ACT1* is deleted and, instead, YFP is expressed from the *ACT1* promoter. We isolated a clone, *ACT1*^f-2, with reliably high excision (>75% rapamycin-induced excision as indicated by YFP expression) that was used for the remainder of our studies.

Residual ACT1 in inducible knockout parasites. To correlate knockout phenotypes with the extent of ACT1 depletion, we developed a semiquantitative approach that uses the ACT1 immunofluorescence staining intensity in single parasites as a proxy for ACT1 protein abundance (Fig. 2A). Consistent with a previous report (16), we observed that a large portion of the Δ*act1* parasites retained substantial residual ACT1 2 days after the induction of gene excision (Fig. 2B and C). When assayed 3 days or more after the induction of gene excision, Δ*act1* parasites were much more uniformly depleted of ACT1 relative to the amounts in *ACT1*^f intact controls (Fig. 2B and C). Importantly, at all time points considered, the mean ACT1 staining intensity of Δ*act1* parasites never fell below the low end of ACT1 staining observed in *ACT1*^f intact parasites (Fig. 2B and C). Similar low levels of ACT1 staining were also observed in parasites of the parental *diCre* strain bearing a native *ACT1* locus (Fig. 2B and C), suggesting that these results are unlikely to be an artifact of misclassifying Δ*act1* parasites as *ACT1*^f intact due to low YFP expression. In addition, in every biological replicate and at every time point, even 5 days after inducing gene disruption, a small number of knockout parasites still stained moderately for ACT1 (Fig. 2B and C).

We then asked whether any of the residual ACT1 staining detected in Δ*act1* parasites might actually represent bleed through from the YFP channel or cross-reactivity of the actin antibody. To test for bleed through, we altered our immunostaining protocol to exclude the primary or secondary antibodies used to detect ACT1.
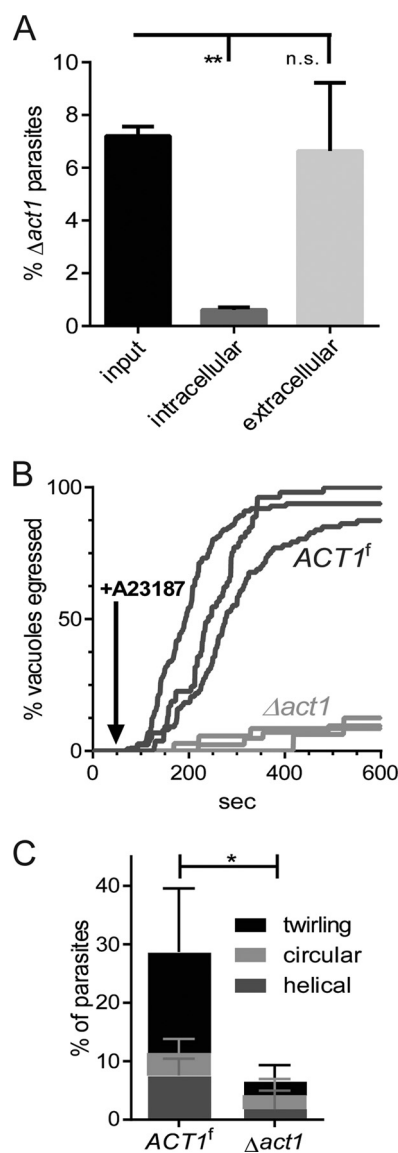
FIG 1 Analysis of actin-dependent motility after deletion of *ACT1*[f]. (A) Invasion efficiency was determined with a differential staining protocol that detects intracellular or extracellular parasites based on protection from SAG1 staining (MAb DG52) prior to permeabilization and differentiates between *ACT1*[f] intact and Δ*act1* parasites based on YFP expression. The percentages of knockouts in the input, intracellular, and extracellular parasite populations after a 30-min invasion period are shown as the means ± standard deviations (SD) ($n = 3$). **, $P \leq 0.01$; one-way ANOVA with Dunnett's multiple-comparison test; n.s., not significant. The data shown are from 1 of 3 independent experiments, in all of which Δ*act1* parasites were significantly underrepresented among intracellular parasites relative to their representation in the input population. (B) Egress was induced by A23187 and tracked with time-lapse video microscopy. Δ*act1* parasites were identified by YFP expression. Traces show the cumulative percentages of egress by ≥16 vacuoles per sample; each individual trace represents the results of an independent experiment. (C) Parasite gliding on serum-coated coverslips was observed by time-lapse video microscopy; Δ*act1* parasites were identified by YFP expression. Columns show mean percentages of parasites ± SD from 3 independent experiments, for each of which 25 to 60 Δ*act1* parasites were scored. *, $P \leq 0.05$; one-way ANOVA. All experiments were performed 2 days after rapamycin-induced excision of *ACT1*[f] in the previously described *ACT1*[f]-1 strain (15).

These alterations strongly reduced the signal observed in the ACT1 channel, suggesting that the original signal detected using *T. gondii* ACT1 (TgACT1) antibody was only minimally influenced by channel bleed through (see Fig. S2 in the supplemental material). Replacing our TgACT1 antibody with rabbit IgG antiserum as an isotype control also significantly reduced the observed signal, although not as strongly as exclusion of primary or secondary antibodies (Fig. S2). Unlike the TgACT1 staining in Δ*act1* parasites, the mean signal observed using this isotype control was below the range of TgACT1 staining observed in *ACT1*[f] intact parasites. Thus, some but not all of the residual staining with TgACT1 in Δ*act1* parasites may derive from a low level of reactivity of rabbit antisera against parasites. Because of the low reactivity of rabbit antisera against parasites, we further tested the specificity of the residual ACT1 staining by using a mouse monoclonal antibody (MAb) raised against *Dictyostelium* actin. Using this monoclonal antibody, we again observed substantial residual ACT1 staining in Δ*act1* parasites (Fig. 2B), again suggesting that the observed signal does indeed reflect residual ACT1 in Δ*act1* parasites.

The consistent presence of residual ACT1 in some portion of Δ*act1* parasites, combined with the prior observation that *Toxoplasma* ACT1 polymerizes isodesmically with no detectable critical concentration (22), led us to hypothesize that trace ACT1 retained by Δ*act1* parasites may suffice to support the limited invasion observed after gene disruption. Under this model, we would predict that the longer parasites were maintained after *ACT1* disruption, the more strongly depleted of protein they would be and the more severe defects in invasion would become. To test this, we used our modified invasion assay to determine the severity of the invasion defect in parasites maintained for 2 to 5 days after rapamycin induction of *ACT1*[f] excision. As predicted, the strength of Δ*act1* parasites' invasion defect correlated positively with the length of time parasites were maintained after the induction of gene excision (Fig. 3A).

If residual ACT1 is responsible for the continued ability of some Δ*act1* parasites to invade host cells, we would expect that ACT1 would still be detectable in Δ*act1* parasites following invasion. To test this, we quantified the levels of ACT1 immunofluorescence staining intensity in confocal images of parasites that were allowed to newly invade fibroblasts 4 days after rapamycin induction of *ACT1*[f] excision. In this experiment, we observed no significant differences in the ACT1 content of intracellular or extracellular parasites, although Δ*act1* parasites were again on average depleted of ACT1 relative to the amounts in *ACT1*[f] intact parasites (Fig. 3B). Importantly, there was substantial overlap in the ACT1 staining intensities observed in individual Δ*act1* and *ACT1*[f] parasites, again consistent with a model of residual ACT1 facilitating Δ*act1* parasite invasion (Fig. 3B).

Sensitivity of invasion to actin polymerization inhibitors. Parasite invasion is known to be sensitive to the actin polymerization inhibitor cytochalasin D (CytD) (2). If Δ*act1* parasites rely on residual ACT1 for invasion, we reasoned that these Δ*act1* parasite invasions would retain CytD sensitivity. To test this, we used our modified invasion assay to track parasite invasion into both human foreskin fibroblast (HFF) cells and a CytD-resistant epithelial cell line, Cyt-1 (24). Four days after the induction of gene excision, we observed dose-dependent CytD inhibition of invasion into HFF cells by both *ACT1*[f] intact and Δ*act1* parasites, confirming that invasion by Δ*act1* parasites is indeed actin dependent
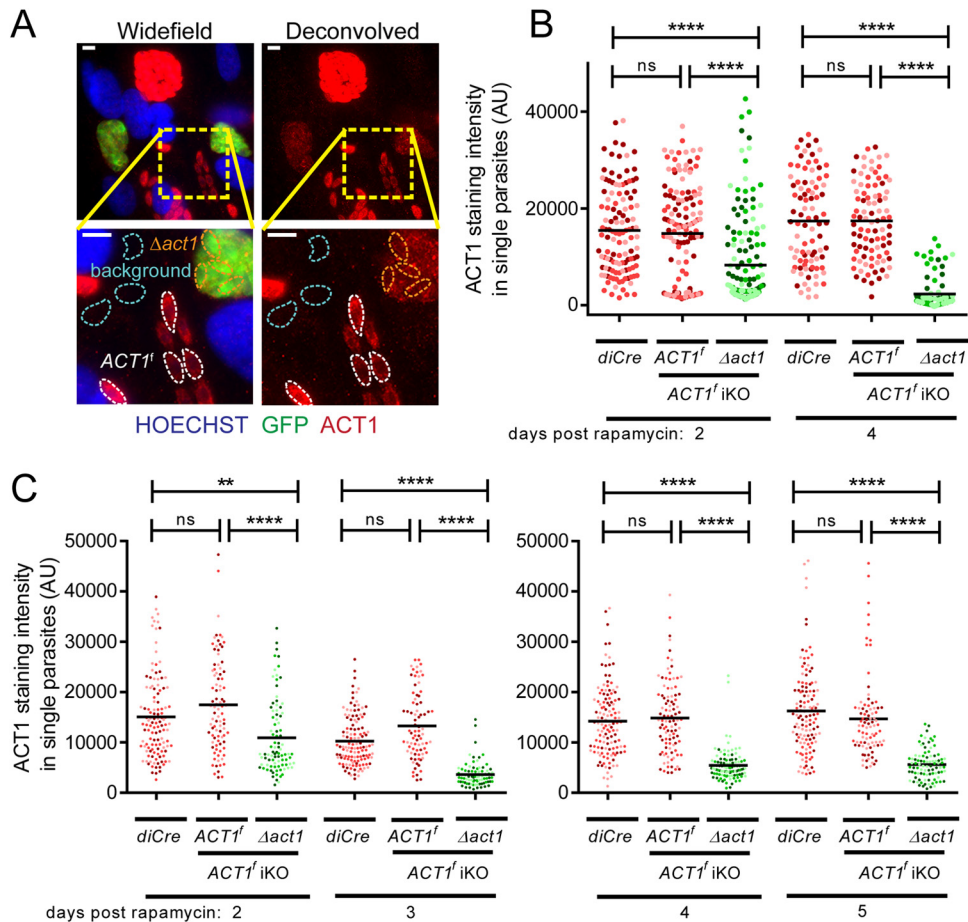
FIG 2 Estimating ACT1 abundance after gene excision. (A) ACT1 abundance was estimated by measuring immunofluorescence staining intensity. Individual parasites were traced in deconvolved Z series images to quantify anti-TgACT1 antibody staining intensity. Δact1 parasites were identified by YFP expression, as indicated by anti-GFP antibody staining. The mean signal from 5 host cytosol regions within the same field of view was used for background subtraction. Images depict an example of a field containing both ACT1^f and Δact1 parasites 4 days after induction of gene excision. Scale bars = 5 μm. (B and C) Quantification of ACT1 staining intensities in ACT1^f-2 and the parental diCre strain 2 to 5 days after rapamycin induction of ACT1^f excision (iKO [inducible knockout strain]). ACT1 was stained with either monoclonal anti-Dictyostelium actin antibody (B) or polyclonal anti-TgACT1 antibody (C). Three separate cultures were induced in parallel; different color intensities denote results for parasites from different biological replicates. Dots indicate background-subtracted fluorescence intensities from single parasites, expressed in arbitrary units (AU), and lines show mean intensities. **, $P \leq 0.01$; ****, $P \leq 0.0001$; Kruskal-Wallis test with Dunn's multiple-comparison test. All experiments were performed with a newly derived inducible ACT1 knockout mutant, ACT1^f-2.

(Fig. 4A). CytD is a reversible inhibitor of actin polymerization. Because Δact1 parasites contain less ACT than ACT1^f intact parasites, we predicted that Δact1 parasites would be inhibited at lower CytD concentrations than ACT1^f intact parasites. Consistent with this prediction, when invading HFF cells, Δact1 parasites were inhibited by 200 nM CytD in 3 independent experiments, while ACT1^f intact parasites never showed significant sensitivity below 500 nM CytD (Fig. 4A).

We then asked whether, in the case of Δact1 parasite invasion, CytD sensitivity might reflect inhibition of an actin-dependent pathway in the host. This possibility was tested by analyzing invasion into the CytD-resistant epithelial cell line, Cyt-1 (24). For all parasites, invasion into Cyt-1 cells was slightly more CytD sensitive than invasion into HFF cells. This may stem from differing quantities of actin in the host cells altering the effective CytD concentration experienced by the parasites or from the drug affecting host processes that may contribute to invasion. Importantly, however, invasion by both Δact1 and ACT1^f intact parasites into Cyt-1

cells was inhibited by CytD (Fig. 4). Furthermore, parallel invasions by parasites with a CytD-resistant act1^{A136G} allele (2) into both HFF and Cyt-1 cells were not affected at these concentrations of CytD, supporting the ability of our assay to detect a CytD-resistant phenotype. In combination, these results suggest that the major invasion-inhibiting target of CytD is parasite actin rather than host actin, for both Δact1 and ACT1^f intact parasites.

Impact of ACT1 knockout on invasion stages. Finally, we asked if it was possible to delineate roles for ACT1 in specific stages of invasion. We first considered the attachment of parasites to HFF cells rendered too rigid for invasion by glutaraldehyde fixation. When a mixed population of ACT1^f intact and Δact1 parasites were allowed to attach to glutaraldehyde-fixed HFF cells, Δact1 parasites were similarly abundant among the input parasite population and attached parasites, indicating that ACT1 disruption does not inhibit the initial attachment stages of invasion (Fig. 5A). We then used a short (90 s) invasion pulse and staining for the MJ marker RON4 to determine whether Δact1 parasites
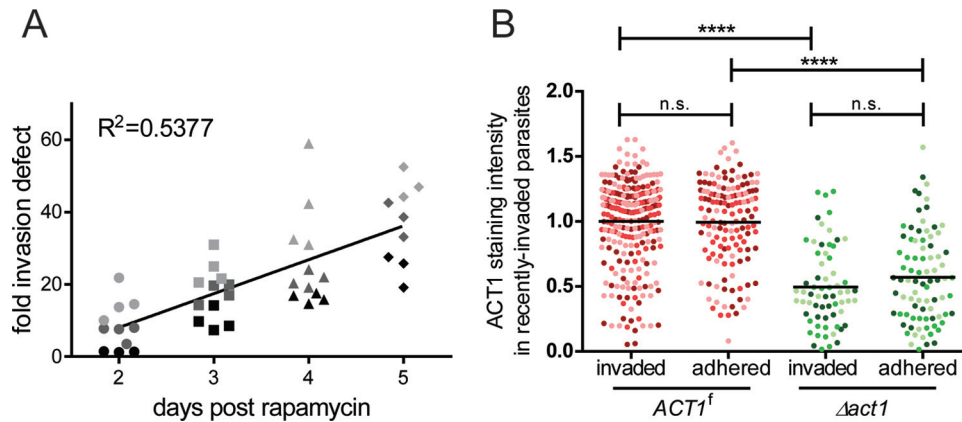
FIG 3 Residual ACT1 levels and invasion by Δ*act1* parasites. (A) The magnitude of the invasion defect of Δ*act1* parasites was determined at different time points after rapamycin-induced *ACT1* excision. The invasion defect was quantified by comparing the frequency of Δ*act1* parasites among intracellular parasites after a 30-min invasion to their abundance in the initial parasite population using the following equation: fold invasion defect = (% Δ*act1* parasites in input population)/(% Δ*act1* parasites in intracellular population). The Δ*act1* parasite frequency was determined using the differential staining protocol described in the legend to Fig. 1. The data shown are from 3 independent experiments, each with 3 or 4 technical replicates. Matched color intensities denote technical replicates from the same experiment. For linear regression, $R^2 = 0.5377$ and $P < 0.0001$, comparing the slope of the regression line to a slope of 0. (B) Four days after induction of gene excision, ACT1 abundance in recently invaded parasites was estimated by measuring staining intensity. Parasites were classified as intracellular or extracellular and as *ACT1*^{f} intact or Δ*act1* using the differential staining protocol described in the legend to Fig. 1. Lines show the mean intensity for each category. Because invading Δ*act1* parasites were relatively rare, data from 3 independent experiments were combined to generate the graph. The intensities from each data set were normalized to the mean intensity of *ACT1*^{f} intact intracellular parasites. Matched color shading indicates data from the same experiment. Results for at least 20 parasites are shown for every category in each experiment. ****, $P \leq 0.0001$; Kruskal-Wallis test with Dunn's multiple-comparison test. All experiments were performed with *ACT1*^{f}-2.

could effectively secrete rhoptry contents and establish an MJ. In these experiments, Δ*act1* parasites were significantly less likely than *ACT1*^{f} intact parasites to have completed penetration (Fig. 5B). Importantly, however, about half of the Δ*act1* parasites detected were apically attached at a focus of RON4 secretion or in the process of actively penetrating a host cell (Fig. 5B), suggesting that the failure of Δ*act1* parasites to invade does not reflect an inability to establish a functional MJ.

Relatively few Δ*act1* parasites were detected as intracellular compared to the number captured in the process of penetration in our MJ assays (Fig. 5B). We hypothesized that this might be because Δ*act1* parasites may either penetrate host cells more slowly than *ACT1*^{f} intact parasites or fail to complete invasion attempts at all. To test this possibility, we used time-lapse video microscopy to observe invasions by *ACT1*^{f} intact and Δ*act1* parasites. About half of the Δ*act1* parasite invasions detected were completed in a time frame similar to that of *ACT1*^{f} intact parasite invasions (Fig. 5C). The detection of some Δ*act1* parasite invasions with normal kinetics is consistent with a model where a portion of the Δ*act1* parasites are not strongly depleted of ACT1 and, thus, are not true phenotypic nulls. However, while nearly all *ACT1*^{f} intact parasite invasions were complete within a minute, almost a third of the Δ*act1* parasite invasions failed to complete within 4 min (Fig. 5C), suggesting that Δ*act1* parasites have a specific defect in the penetration stage of invasion.

DISCUSSION

Here, we sought to evaluate whether limited invasion by inducible Δ*act1* parasites supports a need to revise the current model that invasion requires a parasite actin-dependent myosin motor. Our analyses of invasion, gliding motility, and egress all indicated that gliding motility-dependent behaviors are inhibited but not completely abolished in Δ*act1* parasites 2 days after *ACT1*^{f} excision

(Fig. 1). By quantifying ACT1 abundance in individual parasites, we found that residual ACT1 is detectable in Δ*act1* parasites as many as 5 days after the induction of *ACT1*^{f} excision (Fig. 2). Supporting the functional relevance of this residual ACT1, we observed a positive correlation between the length of time Δ*act1* parasites were propagated after *ACT1*^{f} excision and the severity of the invasion defect observed in Δ*act1* parasites. Consistent with a model where residual ACT1 enables Δ*act1* parasite invasion, both *ACT1*^{f} and Δ*act1* parasites were sensitive to the actin polymerization inhibitor CytD (Fig. 4). We were unable to detect a defect in host cell attachment for Δ*act1* parasites (Fig. 5A). We further found that Δ*act1* parasites were capable of secreting rhoptries and forming functional MJs (Fig. 5B). However, the frequent failure of Δ*act1* parasites to complete invasion attempts within the time period typical for wild-type parasites (Fig. 5C) suggests a requirement for *ACT1*^{f} specific to the penetration stage of invasion.

The initial studies using inducible Δ*act1* parasites found low levels of parasite motility and invasion as many as 4 days after *ACT1*^{f} excision, and interpreted the ability of some knockout parasites to still invade as evidence in support of an ACT1-independent invasion pathway in *T. gondii* (15, 16). In these studies, the conclusion that ACT1 polymerization was ablated in inducible Δ*act1* parasites relied on qualitative estimation of residual ACT1 by immunofluorescence staining and Western blot analysis of pooled parasite extracts, although the sensitivity of this method was not determined (15, 16). In contrast, our quantification of ACT1 content in individual parasites revealed that there is considerable overlap in the ACT1 content of individual Δ*act1* and *ACT1*^{f} intact parasites, even 5 days after *ACT1*^{f} excision (Fig. 2). We were surprised to detect Δ*act1* parasites with moderate levels of ACT1 so long after rapamycin induction of *ACT1*^{f} excision. We speculate that these cases represent either parasites that spontaneously excised *ACT1*^{f} after rapamycin induction or parasites that
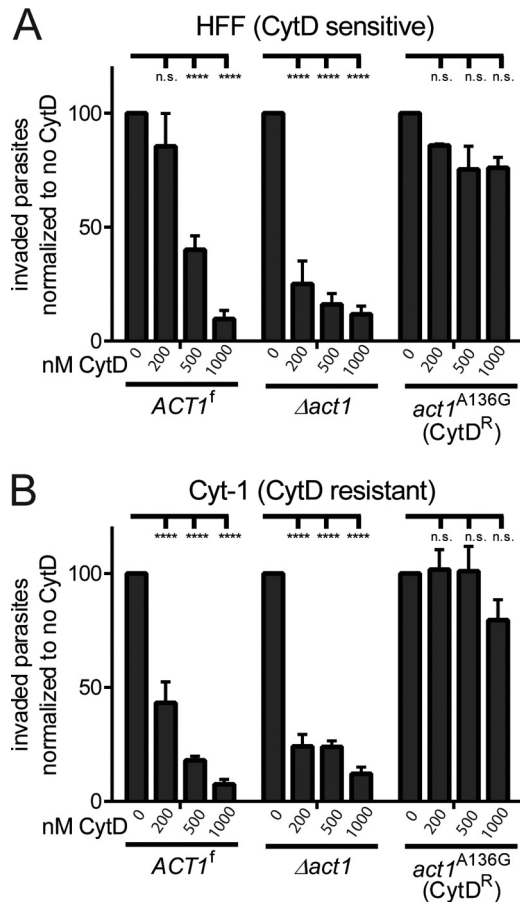
FIG 4 Testing sensitivity of invasion to actin inhibitor cytochalasin D (CytD). (A and B) Parasites were classified as intracellular or extracellular and as *ACT1*[f] intact or Δ*act1* using the differential staining protocol described in the legend to Fig. 1. The invasion rates of *ACT1*[f] intact and Δ*act1* parasites and CytD-resistant *act1*[A136] parasites were compared in CytD-sensitive HFF cells (A) and CytD-resistant Cyt-1 cells (B). Data shown are mean values ± standard errors of the means (SEM) from 3 independent experiments with the *ACT1*[f] parasites and 2 independent experiments with the *act1*[A136] parasites, each with 3 to 5 technical replicates. For each group, the number of intracellular parasites was normalized to the mean invasion rate of that group with no CytD. ****, $P \leq 0.0001$; two-way ANOVA with Dunnett's multiple-comparison test. All experiments were performed with *ACT1*[f]-2 4 days after rapamycin induction of gene excision.

inherited an unusually large portion of the ACT1 mRNA or protein present at the time of *ACT1*[f] excision. Both scenarios are likely rare. However, the fitness defects associated with substantial ACT1 depletion could easily impose a strong selection pressure in favor of any rare Δ*act1* parasites with significant residual ACT1 and, thus, increase their prevalence in the population.

Our subsequent finding that extended propagation of Δ*act1* parasites is correlated with increased severity of the invasion defect supports the role of actin in this process. In accordance with this, the isodesmic polymerization of ACT1 (22) should allow small amounts of residual ACT1 to form filaments and power invasion. We note that the increasing severity of the invasion defect was moderate relative to the expected rapid dilution of ACT1 protein among dividing Δ*act1* parasites. However, quantification of ACT1 levels in Δ*act1* parasites by immunofluorescence assay (IFA) also did not show Δ*act1* parasites becoming dramatically

more depleted of ACT1 beyond day 3. We hypothesize that, upon falling below some required threshold for ACT1 content, Δ*act1* parasites perish and are thus removed from the population.

Further support for the residual ACT1 model is provided by the finding that invasion by inducible Δ*act1* parasites retained sensitivity to the actin polymerization inhibitor CytD. The inability of CytD-resistant host cells to rescue invasion by Δ*act1* parasites demonstrates that CytD is not inhibiting invasion by acting on a host actin-dependent pathway. Rather, CytD inhibits the invasion of Δ*act1* parasites by acting on a parasite target, presumably ACT1, which exhibits CytD-sensitive filament assembly *in vitro* (21). We cannot, however, exclude the possibility that CytD might target some other protein in Δ*act1* parasites, such as the previously described actin-like proteins encoded by *T. gondii* (25).

When considering the invasion stages that ACT1 depletion may affect, we did not detect a defect in the attachment of Δ*act1* parasites to glutaraldehyde-fixed host cells. After attaching to host cells, invading parasites go on to secrete rhoptry proteins and penetrate through an MJ (4). A previous study reported that Δ*act1* parasites overwhelmingly fail to secrete rhoptries or form MJs and hypothesized that this MJ formation defect is primarily responsible for the failure of Δ*act1* parasites to invade host cells (16). When we analyzed MJ formation, we also found that Δ*act1* parasites were less efficient at invasion. However, we observed that nearly half of the Δ*act1* parasites attached to host cells had already secreted rhoptries or even begun penetrating into the host cell (Fig. 5B). Our results suggest that many Δ*act1* parasites are able to form functional MJs but are inhibited at a later step in the invasion process. The discrepancy in these results may stem from methodological differences between the studies. Specifically, our assay used a much shorter invasion pulse (90 s versus 5 min), designed to capture a greater number of parasites still in the process of invading (~2-fold more). However, given the discrepancy between these results and their respective interpretations, we wished to further probe the potential defect of Δ*act1* parasites in invasion stages following attachment and MJ formation. Our subsequent finding that Δ*act1* parasites often fail to complete invasion within the time period typical for *ACT1*[f] intact parasites, as determined by video microscopy, serves as further evidence that Δ*act1* parasites have a defect specific to the penetration stage of invasion.

In total, our results are consistent with a model where ACT1 is essential for efficient penetration of *T. gondii* into host cells. Under this model, inducible knockout of *ACT1* leads to depletion of ACT1 protein and corresponding defects in invasion and other gliding motility-dependent processes. However, because *ACT1* deletion is ultimately lethal to *T. gondii*, generating populations of Δ*act1* parasites that are true phenotypic nulls is not feasible. Instead, Δ*act1* parasite populations generated by Cre-mediated excision of *ACT1*[f] contain parasites that, although Δ*act1* by genotype, still retain functionally relevant quantities of ACT1. Because these parasites with residual ACT1 are present in Δ*act1* parasite populations, invasion is able to continue, albeit at a reduced level. Notably, our results do not exclude the possible existence of additional pathways that could contribute to *T. gondii* invasion. However, the existence of such alternative pathways is not necessary to explain the phenotype of Δ*act1* parasites. Moreover, any such alternative pathways seem unlikely to be major contributors to *T. gondii* invasion, as they are not able to offer a robust or efficient alternative to ACT1-dependent invasion, as evidenced by the major invasion defects of Δ*act1* parasites.
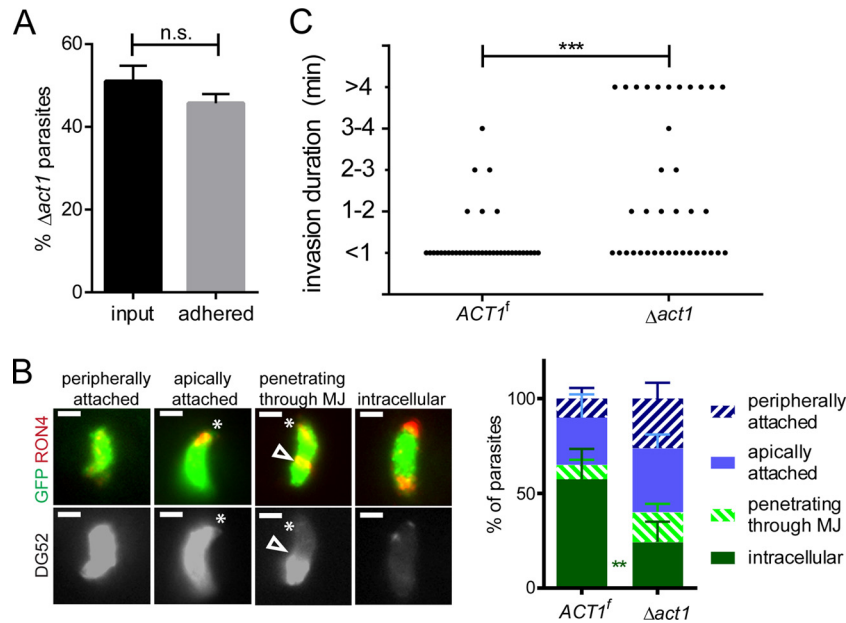
FIG 5 Effect of *ACT1* deletion on adhesion and invasion efficiency. (A) The efficiency of attachment to gluteraldehyde-fixed HFF cells by Δ*act1* parasites relative to that of *ACT1*[f] intact parasites was determined 4 days after rapamycin-induced *ACT1* excision. Δ*act1* parasites were identified by YFP expression, and an aliquot of the input parasites was used to determine Δ*act1* parasite abundance prior to attachment. n.s., $P > 0.05$, unpaired *t* test. Data from 1 of 3 independent experiments, each with 3 to 4 technical replicates, are shown. In all 3 experiments, no significant differences in Δ*act1* parasite frequencies in input and adhered parasite populations were observed. (B) Moving junction (MJ) formation was analyzed by immunostaining after a 90-s invasion pulse. Parasites were classified as peripherally attached or apically attached based on detection of secreted RON4, as penetrating based on partial SAG1 (MAb DG52) protection and the presence of RON4 rings, and as intracellular based on protection from SAG1 (MAb DG52) staining preceding permeabilization. Images show representative Δ*act1* parasites from each category. White asterisks indicate apical ends. White arrowheads indicate the MJ. Scale bars = 2 μm. Data shown are means ± SEM from 3 independent experiments, each with 3 technical replicates. **, $P \leq 0.01$; two-way ANOVA with Sidak's multiple-comparison test. (C) Speed of invasion was determined with time-lapse video microscopy 4 days after *ACT1* excision, using YFP expression to classify parasites as Δ*act1*. Each dot represents a single invasion event. Data from 16 independent experiments were pooled. ***, $P \leq 0.001$; Mann-Whitney test. All experiments were performed with *ACT1*[f]-2 4 days after rapamycin induction of gene excision.

The development of inducible Cre-Lox genetic tools for *T. gondii* (15) offers an exciting opportunity to dissect essential processes. In particular, inducible Cre-Lox technology has facilitated the deletion of several genes thought to encode essential components of the invasion machinery (15–17). For some of these genes, residual invasive ability can be explained by functional redundancies built into the *T. gondii* genome (19, 20). For other, truly essential genes, such as actin, our results highlight the importance of considering the functional implications of residual protein retained in mutants after inducible gene knockout.

MATERIALS AND METHODS

Parasite strains and growth conditions. Parasites were passaged as tachyzoites in human foreskin fibroblast (HFF) cell monolayers as previously described (6). An RH Δ*ku80*::*diCre* strain (15), referred to herein as the *diCre* strain, was used as a wild-type control strain and to generate the new inducible *ACT1* knockout mutant. The initial experiments used a previously described inducible *ACT1* knockout strain, diCre-Act1 (15), referred to herein as *ACT1*[f]-1. Subsequent experiments used a new inducible *ACT1* knockout strain, *ACT1*[f]-2, created as described below. In both *ACT1*[f] strains, excision was induced by treating partially lysed (50 to 75%) parasite cultures with 50 nM rapamycin for 4 h. Induced parasites were isolated by filtration through 3.0-μm filters (Nuclepore), washed twice by dilution in HHE (Hanks' balanced salt solution supplemented with 1 M HEPES and 0.1 M EGTA) and centrifugation at $400 \times g$ to remove any residual rapamycin, and then used to infect fresh HFF cell monolayers. Mixed populations of *ACT1*[f] intact and Δ*act1* parasites were isolated by mechanical lysis of partially lysed cultures, typically 40 to 48 h after inoc-

ulation. To culture Δ*act1* parasites for 4 to 5 days, cultures were mechanically lysed 2 days after induction and reinfected into HFF cells at high doses to compensate for low invasion rates.

Generation of new inducible *ACT1* knockout strain. The plasmids and oligonucleotides used in this study are listed in Table S1 in the supplemental material. To generate the high-excision-rate *ACT1*[f]-2 strain, a plasmid (pLD-03) was constructed with the *ACT1* coding sequence (CDS) flanked by a *Toxoplasma*-specific Kozak sequence (GGCAAA) and LoxP site immediately 5′, and 3′ by a LoxP site followed by a YFP reporter and the HXPGRT selectable marker. To this end, the LoxP-flanked 3′ untranslated region (UTR) of *ACT1* was amplified from RH genomic DNA and ligated into the plasmid pG265, generating the plasmid pLD-02. Gibson assembly of the *ACT1* 3′ UTR preceded by YFP and HXPGRT, isolated from pLD-02 by PacI and ApaI digestion, and the *ACT1* 5′ UTR and CDS fragments, amplified from genomic DNA, was then used to generate pLD-03. The resulting ACT1-floxing cassette was then released from pLD-03 by PvuII digestion to expose the 5′ and 3′ ends of the construct for homologous recombination, and electroporated into the *diCre* strain. After selection with 25 μg/ml mycophenolic acid and 50 μg/ml xanthine (Sigma-Aldrich, St. Louis, MO), parasite clones were isolated by limiting dilution in 96-well plates containing HFF cell monolayers. Clones were screened with both diagnostic PCR (Fig. S1) and dual ACT1/YFP immunostaining after rapamycin treatment to obtain *ACT1*[f]-2, a reliably high-excision-rate inducible knockout strain.

Invasion assay. A previously developed differential staining method was adapted to identify parasites as intracellular or extracellular and as *ACT1*[f] intact or Δ*act1* (26). In this assay, parasites harvested by mechanical lysis were allowed to invade subconfluent HFF cell monolayers on coverslips for 30 min. After thorough rinsing, coverslips were first stained

with DG52, a MAb to SAG1, to mark extracellular parasites. Cell were then permeabilized with 0.05% saponin. After permeabilization, rabbit anti-TgACT1 antibody (12) and rat anti-green fluorescent protein (GFP) antibody (Santa Cruz Biotechnology) were used to identify Δ*act1* parasites by YFP expression. All primary antibodies were recognized by fluorophore-conjugated secondary antibodies (for DG52, Alexa Fluor 594; for TgACT1 antibody, Alexa Fluor 647; and for GFP antibody, Oregon green 488). The slides were imaged on a Cytation3 cell-imaging multimode reader, using Gen5 software for analysis (BioTek, Winooski, VT). All experiments were performed independently at least 3 times, each with 3 to 5 technical replicates.

To determine the abundance of Δ*act1* parasites in input populations, aliquots of the parasites used for invasion were adhered to poly-L-lysine-coated coverslips and then stained with mouse anti-GFP and rabbit anti-TgACT1 antibodies, followed by fluorophore-conjugated secondary antibodies (for GFP antibody, Alexa Fluor 594, and for TgACT1 antibody, Alexa Fluor 488). The slides were visualized on a Zeiss Axioskop 2 MOT plus microscope with an AxioCam MRm monochrome camera and AxioVision software (Carl Zeiss, Inc., Thornwood, NY).

To test the effect of cytochalasin D (CytD) on invasion, parasites were allowed to invade both CytD-sensitive HFF host cells and CytD-resistant Cyt-1 (24) host cells. HFF cells were seeded onto 96-well plates and Cyt-1 cells onto 0.1% gelatin-coated coverslips. Prior to invasion, cells were pretreated for 10 min at room temperature with either CytD or 0.02% dimethyl sulfoxide (DMSO). In experiments testing invasion into HFF cells, only parasites were pretreated with CytD; when testing invasion into the resistant Cyt-1 cells, both parasites and the Cyt-1 cells were pretreated with CytD. After CytD pretreatment, parasites were briefly settled onto host cells by centrifugation at $400 \times g$ and 18°C for 2 min and then allowed to invade for 12 min at 37°C. The same differential staining approach described above was used, except that Cyt-1 cells were permeabilized with 0.25% Triton X-100.

Time-lapse microscopy of egress, gliding, and invasion. To observe egress, parasites were infected onto HFF cell monolayers on glass-bottom culture dishes (MatTek, Ashland, MA) and cultured for 2 days. Immediately prior to the experiment, the monolayers were rinsed twice with Ringer's medium (155 mM NaCl, 3 mM KCl, 2 mM CaCl$_2$, 1 mM MgCl$_2$, 3 mM NaPO$_4$, 10 mM HEPES, 10 mM D-glucose, pH 7.4). To induce egress, 2 μM A23187 was added 30 s into the 10-min-total acquisition periods, during which alternating bright-field and fluorescence images were captured at ~2 frame/5 s, using the Zeiss Axio observer Z1 imaging system and Zen software as previously described (27).

Gliding motility was observed with video microscopy as previously described (27), except that dishes were precoated with 50% fetal bovine serum. Alternating bright-field and FITC fluorescence images were acquired at ~1 frame/3 s. Data from multiple videos taken on the same day were pooled so that 25 to 60 Δ*act1* parasites were analyzed for every experiment, with *ACT1*[f] intact parasites from the same videos serving as control.

Invasion was monitored with video microscopy as previously described (27), except that cells were imaged in dishes containing indicator-free Dulbecco modified Eagle medium (DMEM) (product code D5030; Sigma-Aldrich) supplemented with 1 g/liter glucose, 25 mM HEPES, and 3% fetal bovine serum (FBS) (pH 7.4). Alternating bright-field and FITC fluorescence images were acquired for 10-min periods at ~3 frame/1 s. Invasion duration was defined as the length of time parasites displayed visible moving junctions. To analyze the rare Δ*act1* invasion events, data from 16 independent experiments were pooled, and randomly selected invasions by *ACT1*[f] intact parasites from the same days used as control.

Quantification of ACT1 abundance by IFA. ACT1 staining intensity was used as a semiquantitative proxy for ACT1 protein abundance. Parasite-infected HFF cell monolayers were fixed with 4% formaldehyde and subjected to permeabilization with 0.05% saponin and immunostaining. When considering only ACT1 and YFP expression, ACT1 was stained with rabbit anti-TgACT1 antibody and YFP with mouse anti-GFP anti-

body, followed by fluorophore-conjugated secondary antibodies (for TgACT1 antibody, Alexa Fluor 594, and for YFP antibody, Alexa Fluor 488). For these experiments, 0.25-μm Z series of images were acquired on a Zeiss Axioskop 2MOT Plus microscope and deconvolved with a nearest-neighbor algorithm in AxioVision software. When distinguishing intracellular and extracellular parasites in addition to ACT1 and YFP expression, cells were stained with the GFP/TgACT1/DG52 antibody combinations used in the modified invasion assay. For these experiments, images were acquired on a Zeiss LSM 510 META confocal laser scanning microscope using LSM Image Examiner software. In all experiments, at least 20 parasites were measured for every reported category. To quantify ACT1 staining in images generated by either method, individual parasites were manually traced and fluorescence signals were quantified using Volocity software (PerkinElmer, Waltham, MA). The mean signal of 5 host cytosol regions within the same field of view was used for background subtraction.

Attachment assay. Confluent HFF cell monolayers in 96-well plates were fixed for 10 min in 2% glutaraldehyde to generate rigid, impenetrable host cells. Once fixed, HFF cells were rinsed in phosphate-buffered saline (PBS) and quenched overnight in 1 M glycine. The day of the assay, the fixed HFF cells were rinsed in D3 (DMEM supplemented with 3% FBS, 2 mM glutamine, 10 μg/ml gentamicin, 44 mM sodium bicarbonate, and 10 mM HEPES), equilibrated for at least 1 h in D3 at 37°C, and then transferred to invasion medium (DMEM supplemented with 3% FBS and 25 mM HEPES) immediately before the assay. After briefly settling parasites into each well with 2 min of centrifugation at $400 \times g$, attachment was carried out for 15 min at 37°C. Unattached parasites were then removed by rinsing wells 10 times with room temperature PBS. Live parasites attached to the glutaraldehyde-fixed HFF cells were immediately imaged, using the Zeiss Axio Observer Z1 imaging system with Zen software (Carl Zeiss, Inc., Thornwood, NY) and an ORCA-ER digital camera (Hamamatsu Photonics, Japan) to generate bright-field and fluorescence images. Eighty to 200 parasites, split among at least 2 separate fields of view, were analyzed for each well. Bright-field and FITC images of control aliquots of parasites spun directly into HFF cell-free wells were used to determine the abundance of YFP-expressing Δ*act1* parasites in the input population.

Moving junction assay. After harvesting by mechanical lysis, parasites were transferred to intracellular buffer (5 mM NaCl, 142 mM KCl, 1 mM MgCl$_2$, 2 mM EGTA, 5.6 mM D-glucose, 25 mM HEPES, pH 7.4) and allowed to invade subconfluent HFF cell monolayers on coverslips in 24-well plates for 90 s. The 24-well plates were then immediately transferred to an ice water bath. Coverslips were rinsed, fixed with 4% formaldehyde, and processed for immunofluorescence. To mark extracellular parasites, cells were stained with MAb DG52 prior to permeabilization with 0.05% saponin. After permeabilization, anti-GFP antibody was used to mark Δ*act1* parasites, a rabbit polyclonal antibody to RON4 provided by John Boothroyd was used to mark the moving junction, and fluorophore-conjugated secondary antibodies (for DG52, Alexa Fluor 350; for GFP antibody, Alexa Fluor 488; and for RON4 antibody, Alexa Fluor 594) were used for visualization. Images were acquired on a Zeiss Axioskop 2MOT plus microscope, using an AxioCam MRm monochrome camera and AxioVision software (Carl Zeiss, Inc., Thornwood, NY).

Statistics. All statistical tests were performed in Prism (Graph-Pad Software, Inc., La Jolla, CA). Unless otherwise noted, data sets were assumed to be normally distributed and were analyzed with repeated-measures one-way analysis of variance (ANOVA) if considering only a single independent variable (e.g., genotype alone) and two-way ANOVA if considering two independent variables (e.g., genotype and CytD). To compare individual means within an ANOVA, Dunnett's multiple comparison test was used if comparing all means against a single control and Sidak's multiple-comparison test if comparing selected pairs of means. ACT1 staining intensity data sets were not normally distributed and, therefore, were analyzed using a nonparametric Kruskal-Wallis test, with

Dunn's multiple-comparison test for selected groups. To accommodate noncomplete invasion events, invasion duration data were treated as ordinal and analyzed with a Mann-Whitney test. All posttests used corrections for multiple comparisons. In all cases, two-tailed *P* values were calculated, and a *P* value of ≤0.05 was considered significant.

SUPPLEMENTAL MATERIAL

Supplemental material for this article may be found at http://mbio.asm.org/lookup/suppl/doi:10.1128/mBio.00557-15/-/DCSupplemental.

Table S1, PDF file, 0.1 MB.
Figure S1, PDF file, 0.3 MB.
Figure S2, PDF file, 0.2 MB.

REFERENCES

1. **Sibley LD**. 2010. How apicomplexan parasites move in and out of cells. Curr Opin Biotechnol **21:**592–598. http://dx.doi.org/10.1016/j.copbio.2010.05.009.
2. **Dobrowolski JM, Sibley LD**. 1996. Toxoplasma invasion of mammalian cells is powered by the actin cytoskeleton of the parasite. Cell **84:**933–939. http://dx.doi.org/10.1016/S0092-8674(00)81071-5.
3. **Meissner M, Schlüter D, Soldati D**. 2002. Role of Toxoplasma gondii myosin A in powering parasite gliding and host cell invasion. Science **298:**837–840. http://dx.doi.org/10.1126/science.1074553.
4. **Shen B, Sibley LD**. 2012. The moving junction, a key portal to host cell invasion by apicomplexan parasites. Curr Opin Microbiol **15:**449–455. http://dx.doi.org/10.1016/j.mib.2012.02.007.
5. **Besteiro S, Dubremetz J-F, Lebrun M**. 2011. The moving junction of apicomplexan parasites: a key structure for invasion. Cell Microbiol **13:**797–805. http://dx.doi.org/10.1111/j.1462-5822.2011.01597.x.
6. **Morisaki JH, Heuser JE, Sibley LD**. 1995. Invasion of Toxoplasma gondii occurs by active penetration of the host cell. J Cell Sci **108:**2457–2464.
7. **Carruthers V, Boothroyd JC**. 2007. Pulling together: an integrated model of Toxoplasma cell invasion. Curr Opin Microbiol **10:**83–89. http://dx.doi.org/10.1016/j.mib.2006.06.017.
8. **Carruthers VB, Sibley LD**. 1997. Sequential protein secretion from three distinct organelles of Toxoplasma gondii accompanies invasion of human fibroblasts. Eur J Cell Biol **73:**114–123.
9. **Lebrun M, Michelin A, El Hajj H, Poncet J, Bradley PJ, Vial H, Dubremetz JF**. 2005. The rhoptry neck protein RON4 re-localizes at the moving junction during Toxoplasma gondii invasion. Cell Microbiol **7:**1823–1833. http://dx.doi.org/10.1111/j.1462-5822.2005.00646.x.
10. **Alexander DL, Mital J, Ward GE, Bradley P, Boothroyd JC**. 2005. Identification of the moving junction complex of Toxoplasma gondii: a collaboration between distinct secretory organelles. PLoS Pathog **1:**e17. http://dx.doi.org/10.1371/journal.ppat.0010017.
11. **Ryning FW, Remington JS**. 1978. Effect of cytochalasin D on Toxoplasma gondii cell entry. Infect Immun **20:**739–743.
12. **Dobrowolski JM, Niesman IR, Sibley LD**. 1997. Actin in the parasite Toxoplasma gondii is encoded by a single copy gene, ACT1 and exists primarily in a globular form. Cell Motil Cytoskeleton **37:**253–262. http://dx.doi.org/10.1002/(SICI)1097-0169(1997)37:3<253::AID-CM7>3.0.CO;2-7.
13. **Gonzalez V, Combe A, David V, Malmquist NA, Delorme V, Leroy C,** **Blazquez S, Ménard R, Tardieux I**. 2009. Host cell entry by Apicomplexa parasites requires actin polymerization in the host cell. Cell Host Microbe **5:**259–272. http://dx.doi.org/10.1016/j.chom.2009.01.011.
14. **Delorme-Walker V, Abrivard M, Lagal V, Anderson K, Perazzi A, Gonzalez V, Page C, Chauvet J, Ochoa W, Volkmann N, Hanein D, Tardieux I**. 2012. Toxofilin upregulates the host cortical actin cytoskeleton dynamics, facilitating Toxoplasma invasion. J Cell Sci **125:**4333–4342. http://dx.doi.org/10.1242/jcs.103648.
15. **Andenmatten N, Egarter S, Jackson AJ, Jullien N, Herman J-P, Meissner M**. 2013. Conditional genome engineering in Toxoplasma gondii uncovers alternative invasion mechanisms. Nat Methods **10:**125–127. http://dx.doi.org/10.1038/nmeth.2301.
16. **Egarter S, Andenmatten N, Jackson AJ, Whitelaw JA, Pall G, Black JA, Ferguson DJ, Tardieux I, Mogilner A, Meissner M**. 2014. The toxoplasma acto-MyoA motor complex is important but not essential for gliding motility and host cell invasion. PLoS One **9:**e91819. http://dx.doi.org/10.1371/journal.pone.0091819.
17. **Bargieri DY, Andenmatten N, Lagal V, Thiberge S, Whitelaw JA, Tardieux I, Meissner M, Ménard R**. 2013. Apical membrane antigen 1 mediates apicomplexan parasite attachment but is dispensable for host cell invasion. Nat Commun **4:**2552. http://dx.doi.org/10.1038/ncomms3552.
18. **Mital J, Meissner M, Soldati D, Ward GE**. 2005. Conditional expression of Toxoplasma gondii apical membrane antigen-1 (TgAMA1) demonstrates that TgAMA1 plays a critical role in host cell invasion. Mol Biol Cell **16:**4341–4349. http://dx.doi.org/10.1091/mbc.E05-04-0281.
19. **Lamarque MH, Roques M, Kong-Hap M, Tonkin ML, Rugarabamu G, Marq J-B, Penarete-Vargas DM, Boulanger MJ, Soldati-Favre D, Lebrun M**. 2014. Plasticity and redundancy among AMA-RON pairs ensure host cell entry of Toxoplasma parasites. Nat Commun **5:**4098. http://dx.doi.org/10.1038/ncomms5098.
20. **Frénal K, Marq J-B, Jacot D, Polonais V, Soldati-Favre D**. 2014. Plasticity between MyoC− and MyoA-glideosomes: an example of functional compensation in Toxoplasma gondii invasion. PLoS Pathog **10:**e1004504. http://dx.doi.org/10.1371/journal.ppat.1004504.
21. **Sahoo N, Beatty W, Heuser J, Sept D, Sibley LD**. 2006. Unusual kinetic and structural properties control rapid assembly and turnover of actin in the parasite Toxoplasma gondii. Mol Biol Cell **17:**895–906. http://dx.doi.org/10.1091/mbc.E05-06-0512.
22. **Skillman KM, Ma CI, Fremont DH, Diraviyam K, Cooper JA, Sept D, Sibley LD**. 2013. The unusual dynamics of parasite actin result from isodesmic polymerization. Nat Commun **4:**2285. http://dx.doi.org/10.1038/ncomms3285.
23. **Brossier F, Jewett TJ, Lovett JL, Sibley LD**. 2003. C-terminal processing of the toxoplasma protein MIC2 is essential for invasion into host cells. J Biol Chem **278:**6229–6234. http://dx.doi.org/10.1074/jbc.M209837200.
24. **Toyama S, Toyama S**. 1988. Functional alterations in beta'-actin from a KB cell mutant resistant to cytochalasin B. J Cell Biol **107:**1499–1504. http://dx.doi.org/10.1083/jcb.107.4.1499.
25. **Gordon JL, Sibley LD**. 2005. Comparative genome analysis reveals a conserved family of actin-like proteins in apicomplexan parasites. BMC Genomics **6:**179. http://dx.doi.org/10.1186/1471-2164-6-179.
26. **Buguliskis JS, Brossier F, Shuman J, Sibley LD**. 2010. Rhomboid 4 (ROM4) affects the processing of surface adhesins and facilitates host cell invasion of Toxoplasma gondii. PLoS Pathog **6:**e1000858. http://dx.doi.org/10.1371/journal.ppat.1000858.
27. **Shen B, Buguliskis JS, Lee TD, Sibley LD**. 2014. Functional analysis of rhomboid proteases during Toxoplasma invasion. mBio **5(5):**e01795-14. http://dx.doi.org/10.1128/mBio.01795-14.
28. **Lourido S, Tang K, Sibley LD**. 2012. Distinct signalling pathways control Toxoplasma egress and host-cell invasion. EMBO J **31:**4524–4534. http://dx.doi.org/10.1038/emboj.2012.299.